Synthesis, crystal structure of the ammonium vanadyl oxalatophosphite and its controlled conversion into catalytic vanadyl phosphates

C. Kouvatas, V. Alonzo, T. Bataille, L. Le Polles, Claire Roiland, G. Louarn, E. Le Fur

Synthesis, crystal structure of the ammonium vanadyl oxalatophosphite and its controlled conversion into catalytic vanadyl phosphates

C Kouvatas, V. Alonzo, T. Bataille, L. Le Pollès, C. Roiland, G. Louarn, E. Le Fur*

Ecole Nationale Supérieure de Chimie de Rennes, CNRS, UMR 6226 « Institut des Sciences Chimiques de Rennes », 11 Allée de Beaulieu, CS 50837, 35708 Rennes cedex 7, France

*Corresponding author. Tel.: +33 2 23 23 80 16; fax : +33 2 23 81 99. eric.le-fur@ensc-rennes.fr

An ammonium vanadyl oxalatophosphite has been synthesized by hydrothermal treatment. The formula is $(NH_4)_2(VOHPO_3)_2C_2O_4$ $2.9H_2O$ **(1)**. The crystal structure of the compound has been determined by single crystal X-ray diffraction and solid state Nuclear Magnetic Resonance spectroscopy (NMR). Compound **1** crystallizes in triclinic symmetry with space group *P*-1, a=6.3844(4) Å, b=7.2278(4) Å, c=9.2965(5) Å, α=67.260(4)°, β=72.927(4)°, γ=85.848(3)°. The vanadium phosphite framework consists of infinite chains of corner-sharing vanadium octahedra and hydrogenophosphite tetrahedra. The oxalate groups ensure the connection between the chains. The ammonium ions and the water molecules are located between the anionic $[(VO)_2(HPO_3)_2C_2O_4]^{2-}$ layers. The thermal behaviour of **1** was carefully studied by combining thermogravimetric analyses, *in situ* X-ray diffraction and Infra-Red spectroscopy. The formation of given vanadyl phosphate catalysts was shown to be atmosphere-dependent of $(NH_4)_2(VOHPO_3)_2C_2O_4$ $2.9H_2O$ thermal decomposition.

Graphical Abstract

The new vanadyl oxalatophosphite, $(NH_4)_2(VOHPO_3)_2C_2O_4$ 2.9 H_2O has been prepared hydrothermally and its structure solved by combining single-crystal X-ray diffraction and Solid State NMR. Thermogravimetric studies and variable temperature X-ray diffraction showed the reversible departure of water molecules upon heating. At higher temperature, an adequate redox balance during the thermal decomposition of the material, allows to control

the preparation of different catalytically active phases in the vanadyl phosphate system: ω-$VOPO_4$ and $(VO)_2(P_2O_7)$.

Keywords: oxalatophosphite; vanadium phosphates; hydrothermal synthesis; variable-temperature X-ray diffraction; solid state NMR.

1. Introduction

Vanadium phosphate-based compounds have been the subjects of many works during the recent years due to their catalytic and electrochemical activities finding applications in various fields. For example, vanadyl pyrophosphate and some $VOPO_4$ polymorphs [1] are of great importance in the field of catalysis to product maleic anhydride; the easy redox reactions through the oxidation states of vanadium recently allowed to use vanadium phosphates for energy storage in lithium batteries, such as $LiVPO_4F$ [2, 3] and $Li_3V_2(PO_4)_3$[4].Very lately vanadyl phosphate layers have been assembled to graphene nanosheets to build up supercapacitors composite materials[5, 6]. While phosphate chemistry has been widely explorated[7], phosphite based materials are just emerging as a field of research. Unlike the tetrahedral connectivity through oxygens of the phosphate $(PO_4)^{3-}$ anion, the presence of a terminal H atom onto the phosphorus in the phosphite $(HPO_3)^{2-}$ species reduces the possibility of bonding in a defined spatial area, which can give rise, for example, to very open frameworks[8]. Furthermore, the intrinsic thermal stability of the phosphite groups allows a synthesis and a working temperature for phosphite based materials in a very large range up to at least 400°C.

Most of the vanadium phosphate compounds used in the field of catalysis are generated by thermal decomposition of various precursors. The commonly used vanadyl pyrophosphate $(VO)_2P_2O_7$ is obtained by thermal decomposition of $VOHPO_4$ $½H_2O$[1]. Alternative routes using attractive precursor's methods are currently investigated [9]. Oxalate-based compounds are generally considered as good candidates for the preparation of oxide materials with quite

good achievements[10], due to the readily combustion of the organic part at relatively low temperatures[11].

The study of hybrid organic/inorganic compounds based on vanadophosphates and vanadophosphites mainly focuses on the use of oxalate ligands that act as mono-bidentate or bis-bidentate linkers, resulting in various solids topologies. Most of the structures described in the literature are made of vanadium-oxalato-phosphate or vanadiumoxalato- phosphite layers with cationic species and water molecules occluded between them [12-16] . Such frameworks have been very recently tested as materials for lithium batteries[17-19]. They showed reasonable performances in terms of ionic mobility and thermal stability so that promising results have been obtained for such materials in the field of lithium batteries electrodes [20] [21]. Improvements in this field would beneficiate from accurate structural studies combining XRD, solid state NMR studies and theoretical calculations[22] .

In this context we report on the synthesis of an ammonium vanadyl oxalatophosphite precursor and its thermal behaviour, which has been thoroughly studied by thermogravimetric analyses and variable-temperature X-ray diffraction (VT-XRD). We highlight that it is possible to reach one given vanadyl phosphate catalyst, either vanadium pyrophosphate $(VO)_2P_2O_7$ or some $VOPO_4$ polymorphs, simply in adjusting the reactive atmosphere during the decomposition of the pristine material. Details of the thermal process are here described.

2. Experimental section

2.1 Synthesis

Light green crystals of $(NH_4)_2$ $(VOHPO_3)_2$ C_2O_4 $2.9H_2O$ (**1**) have been obtained by hydrothermal treatment. A mixture of V_2O_5, $(NH_4)_2CO_3$, H_3PO_3, $H_2C_2O_4$ $2H_2O$ and H_2O in the molar ratio 1:8:15:2.8:170 was introduced in a 23 mL capacity Teflon-lined stainless steel Parr hydrothermal reaction vessel and heated at 120 °C for 3 days. After slowly being cooled

down to room temperature, the solid was recovered by vacuum filtration, washed with water, and dried in a desiccant vessel (82 % yield, calculated with respect to vanadium).

2.2 X-ray diffraction

The crystal structure of **1** has been determined by single-crystal X-ray diffraction. The experiments were conducted at room temperature using a four-circle Nonius KappaCCD diffractometer, with graphite monochromated Mo Kα radiation (λ = 0.71073 Å). The intensity data collection was performed through the program COLLECT [23]. The compound structure was solved by direct methods (SIR 97 [24]) and refined by the full matrix least-squares procedure based on F^2, using the SHELXL-97 [25] computer program belonging to the WINGX software package [26].

Crystallographic details for **1** are given in Table S1. Selected bonds lengths and angles are given in Table S2.

2.3 Thermal behaviour

Coupled thermogravimetric and DSC measurements were performed with a TA instruments SDT Q600 thermobalance under both pure nitrogen and air from room temperature to 720°C with a heating rate of 0.68°C/min.

Variable temperature X-ray diffraction (VT-XRD) experiments were performed within a Anton Paar HTK 1200N chamber attached to a Panalytical Empyrean powder diffractometer. (θ–θ Bragg–Brentano geometry) working with the Cu *K*α radiation (λ $K\alpha_1$ = 1.5406 Å, λ $K\alpha_2$ = 1.5444 Å) selected with a flat multilayer X-ray mirror (Bragg-Brentano HD®). Data were collected with a Pixel 1D silicon-strip detector, in the angular range 5–60° (2θ) (step size ~0.013° (2θ). Patterns were collected every 5 °C up to 600 °C, with a heating rate of 1°C min-

[1] -between steps. The decomposition of the precursor was carried out either in air or pure nitrogen, to evaluate the influence of the oxygen on the decomposition scheme.

2.4 NMR spectroscopy

All solid-state NMR spectra were acquired using a Bruker Avance I spectrometer equipped with a 7 T magnet. Larmor frequencies are 121.495 MHz for ^{31}P and 300.13 MHz for ^{1}H. Recycle delays of 10 s and 1s were used, with 160 and 32 scans per spectrum respectively. In all experiments, the recycle delay employed is chosen rather short because of the short relaxation time T1 measured for this compound which is consistent with its paramagnetic nature.

Samples were packed into 4-mm outer diameter zirconia rotors and rotated at spin rates of 14 and 14.5 kHz. Single pulse ^{1}H and ^{31}P experiments were carried out at $\omega_{nut}^{H}/2\pi$ = 69 kHz and $\omega_{nut}^{P}/2\pi$ = 125 kHz (corresponding to a RF pulse duration for a $\pi/2$ pulse of 2 µs and 3.6 µs respectively for ^{31}P and ^{1}H).

The isotropic signals were determined by comparing spectra with different spinning rates for each nucleus (10 and 14 kHz for ^{31}P NMR spectra and 13.5, 14, and 14.5 kHz for ^{1}H NMR spectra) (Fig. S1).

Chemical shift scales are shown relatively to H_3PO_4 1M in aqueous solution and H_2O for ^{31}P and ^{1}H spectra respectively

2.5 Magnetic properties

Magnetic susceptibility measurements were performed on powdered samples (27.7 mg) from 2 to 300 K in an applied field of 5 kOe using a MPMS Quantum Design SQUID magnetometer. After the data were corrected from diamagnetic contributions, the $\chi^{-1} = f(T)$ curve was well fitted with a Curie-Weiss law $\chi = C/(T - \theta)$. The magnetic moment obtained

from the linear part of the curves ($T \geq 10$ K) is in excellent agreement with the theoretical value of 1.73 μ_B expected for tetravalent vanadium (experimental magnetic moment per vanadium ion of 1.70 μ_B). At low temperatures antiferromagnetic interactions are evidenced by the upturn observed on the χ^{-1} vs T curve. (Fig. S2)

2.6 FTIR spectroscopic analysis

The infrared spectra were recorded using a Thermo Scientific Nicolet iS5 FT-IR spectrometer with iD7 ATR accessory. A small amount of the grinded samples was laid down on the diamond crystal. Infrared spectra were recorded from 4000 to 400 cm^{-1}. Omnic software was used to display spectra.

The spectrum exhibits bands corresponding to the vibrations of the phosphite anions, oxalate groups, water and ammonium cations (νP-H :2410 cm^{-1}; νP-O :1000-1100 cm^{-1} ; νC=O: 1660 and 1350 cm^{-1}; νO-H and νN-H: 3000-3600 cm^{-1}).

3. Results and discussion

3.1 Structure description

The structure of **1** reveals some similarities with the ones of ammonium oxalatophosphate described by Do *et al.*[10] and sodium vanadyl oxalatophosphate described by Colin *et al.*[15]. The vanadium atoms are coordinated by six oxygen atoms, forming distorted octahedra classically observed in V^{4+} and V^{5+} chemistry [27]. One oxygen atom has a short V=O bond length corresponding to the vanadyl group (d_{V-O} =1.590(2) Å). Three of the oxygen atoms are shared with three HPO_3 groups with typical distances ranging from 1.992(2) to 2.015(2) Å. The two last oxygen atoms are shared with a C_2O_4 group (d_{V-O} =2.083(2)-2.295(2) Å). The three oxygen atoms in the tetrahedral HPO_3 group are shared with vanadium atoms (d_{P-O} =1.519(2) Å to 1.533(2) Å), and the H atom is terminal with a P-H distance of 1.32(4) Å (Fig.

1a). Three vanadium octahedra are linked together by a HPO_3 group to form infinite chains $[VOHPO_3]_\infty$. The infinite chains are connected to each other by C_2O_4, resulting in layers with the formula $[(VO)_2(HPO_3)_2(C_2O_4)]^{2-}$, as shown in figure 1b.

In **1**, the ammonium cations are in tetrahedral environment: they are surrounded by four oxygen atoms (Fig. S3), two of them coming from water molecules, one from an oxalate group shared with vanadium atoms in a layer and the last one is shared between a vanadium atom and a phosphorus atom in an adjacent layer. The interlayer distance is *ca.* 6.66 Å.

^{31}P and ^{1}H MAS NMR studies give results in agreement with structural model obtained by X-ray single crystal diffraction. (Fig. 2)

Single-pulse ^{31}P MAS NMR experiments were carried out in order to quantitatively reflect the various P populations of the oxalatophosphite. The relatively broad line (total linewidth close to 1000 ppm) observed on the resulting spectrum is consistent with the paramagnetic nature of the compound. Only one isotropic phosphorus NMR signal is obtained at 748 ppm, in agreement with the number of crystallographic sites predicted by the X-ray crystal structure solution (Fig. 2a).

The MAS ^{1}H spectrum shows two isotropic signals at 0.9 ppm and -29.7 ppm. We carefully checked that no other broad signal is hidden under these two narrow lines. One of the signals at -29.7 ppm is quite shifted regarding the one at 0.9 ppm. This large negative shift is presumably induced by the vicinity of a paramagnetic center represented by the vanadium with an oxidation state of +IV, as evidenced by magnetic measurement. Thus the ^{1}H MAS NMR spectrum can describe two types of hydrogen of the oxalatophosphite structure: hydrogen ammonium cations and the water molecules resonating on average at 0.9 ppm, and the proton from the HPO_3 groups connected to the paramagnetic vanadium cations shifted at -29.7 ppm. This assignation is consistent with the integrated intensities of the isotropic signals

at 0.9 ppm and -29.7 ppm after fitting, which are approximately 77% and 23% respectively (Fig. 2b).

3.2 Thermal decomposition

3.2.1 Dehydration process of the precursor

Water molecules departure for **1** is observed on up to *ca.* 100°C, both under N_2 or air atmosphere (Fig. 3). The global weight loss is 11.0%, in agreement with the departure of 2.9 water molecules per chemical formula unit (theoretical: 11.1%). This process occurs into 2 successive losses with an inflexion at 50°C. The first weight loss of ~3.3 % is observed from room temperature up to 50 °C, the second dehydration stage of 7.7 % being from 50 to 100 °C. As regards the hydrogen bonds around the two non-equivalent water molecules (Table 1), as well as their amount into a unit cell (2 Ow1 and 0.9 Ow2 water molecules), it is obvious that Ow2 releases at the lowest temperature. A VT-XRD experiment was performed under flowing air (Fig. 4) up to 130 °C and cooled down to RT. It clearly shows the behaviour of the crystal structure upon dehydration. Below 100 °C, the water loss observed from the TGA is accompanied with a continuous change in the positions of the diffraction peaks, while the crystal structure of the pristine phase is preserved. At *ca.* 100 °C, the phase transition corresponds to the modification of the structure into that of the anhydrous compound, as determined from the TG curve. After cooling down this phase from 130°C to 30 °C in wet atmosphere, the fully hydrated compound is observed again as shown by the unit cell parameters refinement performed on the last powder pattern

3.2.2 Atmosphere-dependent decomposition of the anhydrous phase

As shown in figure 3, the formation of anhydrous $(NH_4)_2(VOHPO_3)_2C_2O_4$ is independent from the atmosphere used. In both cases, this phase is stable up to 190 °C. Under pure

nitrogen, a total weight loss of 34.0% is observed at 720°C corresponding to the decomposition of oxalate and ammonium groups. It gives a global formula $VPO_{4.5}$ (expected value: 34.5%). X-ray powder diffraction performed on the compound heated up to 720°C in pure N_2 shows that an amorphous product is obtained.

In the presence of oxygen (air) a slight increase of the mass is observed at *ca*. 190°C. This suggests an oxidation process according to the presence of the phosphite group [28, 29]. A sample was heated to 210 °C in air and cooled down to RT after few hours. Its IR spectrum was then compared to that of the precursor (Fig. 5). As expected, the band corresponding to the P-H bond [30] at 2410 cm^{-1} decreases while a band, that can be attributed to phosphate group[14], appears at 900 cm^{-1}. Successive powder patterns of $(NH_4)_2(VOHPO_3)_2C_2O_4$ collected at 190°C under airflow allowed us to conclude that the latter slowly transforms into an unknown poorly crystalline compound over 12 hours (Fig S4), in agreement with the expectations. Within the elapsed time of the TGA experiment, the diffraction patterns clearly evidenced that both phosphite and phosphate phases co-exist, which explain that the mass gain does not correspond to the full uptake of one O atom (expected 6.9%). Unit cell dimensions can be proposed for this compound, on the basis of the indexing of the available diffraction lines: a = 6.307(2) Å, b = 8.354(5) Å, c = 8.832(4) Å, β = 102.95(5)° [M_9 = 66, F_9 = 47(0.007, 26)]. Interestingly, there are strong analogies with comparison to that of a previously reported oxalate-phosphate compound with a similar formula, $Na_2(VOHPO_4)_2C_2O_4.(1\text{-}x)H_2O$, i.e., a = 6.39 Å, b = 17.10 Å, c = 5.93 Å, β = 106.1° [15], where the a cell parameter is comparable and the b axis is double that of the present compound. In addition, the three cell lengths are close to that of the precursor.

The decomposition of the oxalate group becomes significant at *ca.* 215 °C to reach a weight loss of 32.0% at 420 °C, achieved in both atmospheres (N_2 and air). At this stage, the sample

is amorphous (Fig. 6). Then, a mass gain of 0.7% is observed in air from 500°C and the final weight loss of 31.3% is in agreement with the general formula VPO_5 (Fig. S5).

If the atmosphere is changed from air to N_2 at 420°C the weight continues decreasing, and a final weight loss of *ca*. 34.2% suggests the formation of the compound $VPO_{4.5}$ (expected value: 34.5%). (Fig. S5).

In situ X-ray powder diffraction performed beyond 400 °C in air shows the crystallization of ω-$VOPO_4$ which appears slowly at 430 °C (Fig. 6a). This observation combined with the weight gain observed during TGA experiment (*vide infra*) confirm a full oxidation ofvanadium and phosphorus to their highest oxidation state. . Under nitrogen $(VO)_2P_2O_7$ crystallizes above 570 °C (Fig. 6b) in agreement with TGA experiment suggesting that only phosphorus atoms are oxidized.

Finally, the thermal studies of the decomposition of $(NH_4)_2(VOHPO_3)_2C_2O_4$ 2.9 H_2O show that a control of the atmosphere allows to prepare different materials: amorphous $VPO_{4.5}$ under N_2, ω-$VOPO_4$, under air and $(VO)_2P_2O_7$ by a 2 steps reaction with first the oxidation of the phosphite group under air atmosphere and second a final heating under nitrogen to avoid the oxidation of vanadium 4+ into vanadium 5+ as depicted in scheme 1.

4. Conclusion

The new vanadyl oxalatophosphite, $(NH_4)_2(VOHPO_3)_2C_2O_4$ 2.9 H_2O has been prepared, its structure solved by single-crystal X-ray diffraction and confirmed by ^{31}P and ^{1}H solid state NMR. Thermogravimetric studies and Variable Temperature X-ray diffraction showed the reversible departure of water molecules during heating and complex decompositions of the title compound in relation with the used atmosphere. In the presence of air the oxidation of phosphite into phosphate is evidenced, contrary to the study performed under nitrogen which shows no weight gain. Consequently, a control of the atmosphere after the oxidation of

phosphite into phosphate gives the possibility to prepare two different catalytically active materials: on the one hand V^{4+} is oxidized to V^{5+} under air and consequently ω-$VOPO_4$ is the stabilized phase at 430°C; on the other hand under nitrogen V^{4+} remains stable and $(VO)_2(P_2O_7)$ crystallizes at 570°C.

Acknowledgments

The authors are indebted with T. Roisnel for X-ray data collection (Centre de DIFfractométrie des rayons X, CDIFX), T. Guizouarn for the magnetic measurements, both from the Université de Rennes1, France. FEDER, Région Bretagne, Rennes Métropole, CG35 and CNRS contributed to the purchase of NMR spectrometers and X-ray powder diffraction diffractometer. This work benefited from a grant from Agence Nationale de la Recherche (ANR MOSAIC 13-BS08-0018-01)

References

1. N. F. Dummer; J. K. Bartley; G. J. Hutchings, in: *Advances in Catalysis*, Academic Press: 2011; Vol. Volume 54, pp 189-247.
2. J.-M. Ateba Mba; C. Masquelier; E. Suard; L. Croguennec, *Chemistry of Materials* **2012,** 24, (6), 1223-1234.
3. J. Barker; R. K. B. Gover; P. Burns; A. Bryan; M. Y. Saidi; J. L. Swoyer, *Journal of Power Sources* **2005,** 146, (1-2), 516-520.
4. S. C. Yin; H. Grondey; P. Strobel; M. Anne; L. F. Nazar, *Journal of the American Chemical Society* **2003,** 125, (34), 10402-10411.
5. C. Wu; X. Lu; L. Peng; K. Xu; X. Peng; J. Huang; G. Yu; Y. Xie, *Nature Communications* **2013,** 4, 2431.
6. K. H. Lee; Y.-W. Lee; S. W. Lee; J. S. Ha; S.-S. Lee; J. G. Son, *Scientific Reports* **2015,** 5, 13696.
7. A. K. Cheetham; G. Ferey; T. Loiseau, *Angewandte Chemie International Edition* **1999,** 38, 3418-3438.
8. H.-Y. Lin; C.-Y. Chin; H.-L. Huang; W.-Y. Huang; M.-J. Sie; L.-H. Huang; Y.-H. Lee; C.-H. Lin; K.-H. Lii; X. Bu; S.-L. Wang, *Science* **2013,** 339, (6121), 811-813.
9. A. A. Rownaghi; Y. H. Taufiq-Yap; F. Rezaei, *Chemical Engineering Journal* **2010,** 165, (1), 328-335.
10. J. Do; R. P. Bontchev; A. J. Jacobson, *Chemistry of Materials* **2001,** 13, 2601.
11. C. Boudaren; J. P. Auffredic; M. Louer; D. Louer, *Chemistry of Materials* **2000,** 12, (8), 2324-2333.
12. Y. M. Tsai; S. L. Wang; C. H. Huang; K. H. Lii, *Inorganic Chemistry* **1999,** 38, 4183-4187.

13. M. F. Tang; K. H. Lii, *Journal of Solid State Chemistry* **2004,** 177, 1912-1918.
14. F. N. Shi; F. A. Almeida Paz; J. Rocha; J. Klinowski; T. Trindade, *Inorganica Chimica Acta* **2005,** 358, 927-932.
15. J. F. Colin; T. Bataille; S. E. Ashbrook; N. Audebrand; L. Le Polles; J. Y. Pivan; E. Le Fur, *Inorganic Chemistry* **2006,** 45, 6034-6040.
16. S. Auguste; V. Alonzo; T. Bataille; L. Le Pollès; W. Cañon-Mancisidor; D. Venegas-Yazigi; E. Le Fur, *Journal of Solid State Chemistry* **2014,** 211, 212-218.
17. M. Nagarathinam; K. Saravanan; E. J. H. Phua; M. V. Reddy; B. V. R. Chowdari; J. J. Vittal, *Angewandte Chemie-International Edition* **2012,** 51, (24), 5866-5870.
18. A. Shahul Hameed; M. Nagarathinam; M. Schreyer; M. V. Reddy; B. V. R. Chowdari; J. J. Vittal, *Journal of Materials Chemistry A* **2013,** 1, (18), 5721-5726.
19. A. S. Hameed; M. V. Reddy; N. Sarkar; B. V. R. Chowdari; J. J. Vittal, *RSC Advances* **2015,** 5, (74), 60630-60637.
20. G. Férey; F. Millange; M. Morcrette; C. Serre; M.-L. Doublet; J.-M. Grenèche; J.-M. Tarascon, *Angewandte Chemie* **2007,** 119, (18), 3323-3327.
21. C. N. R. Rao; S. Natarajan; R. Vaidhyanathan, *Angewandte Chemie International Edition* **2004,** 43, 1466-1496.
22. J. Cuny; J. R. Yates; R. Gautier; E. Furet; E. Le Fur; L. Le Polles, *Magnetic Resonance in Chemistry* **2010,** 48, S171-S175.
23. Nonius, *Kappa CCD Program Software, Nonius BV, Delft, The Netherlands* **1998**.
24. A. Altomare; M. C. Burla; M. Camalli; G. L. Cascarano; C. Giacovazzo; A. Guagliardi; A. G. G. Moliterni; G. Polidori; R. Spagna, *Journal of Applied Crystallography* **1999,** 32, 115.
25. G. M. Sheldrick, *Acta Crystallographica, Section A: Foundations of Crystallography* **2008,** 64, (1), 112-122.
26. L. J. Farrugia, *J. Appl. Cryst.* **1999,** 32, 837-838.
27. M. Schindler; F. C. Hawthorne; W. H. Baur, *Chemistry of Materials* **2000,** 12, (5), 1248-1259.
28. W.-S. Dong; J. K. Bartley; N.-X. Song; G. J. Hutchings, *Chemistry of Materials* **2005,** 17, (10), 2757-2764.
29. F. Hamchaoui; V. Alonzo; D. Venegas-Yazigi; H. Rebbah; E. Le Fur, *Journal of Solid State Chemistry* **2013,** 198, (0), 295-302.
30. S. Auguste; V. Alonzo; T. Bataille; L. Le PollÃ¨s; W. CaÃ±Ã³n-Mancisidor; D. Venegas-Yazigi; E. Le Fur, *Journal of Solid State Chemistry* **2014,** 211, 212-218.

Fig 1: (a) Asymmetric unit of **1**, (b) view of the structure of **1** along the [100] direction. Vanadium polyhedra are in blue, phosphite groups are in yellow, ammonium cations are in pale green and carbon cations are in blue-green, oxygen anions and water molecules are in red and hydrogen cations in grey.

Fig 2: (a) ^{31}P MAS NMR at a spinning rate of 14 kHz showing one signal at 748ppm, suggesting only one phosphorus crystallographic site in agreement with X-ray diffraction and (b) ^{1}H MAS NMR experimental fitted spectrum of $(NH_4)_2(VOHPO_3)_2C_2O_4$,2.9 H_2O at a spinning rate of 14.5 kHz (in blue), showing two isotropic signals at 0.9 ppm and -29.7 ppm.

Fig 3: Thermogravimetric curves for compound **1** under flowing air (full line) and nitrogen (dashed line).

Fig 4: Reversibility of the dehydration of **1** observed by VT-XRPD in air between RT and 130 °C

Fig 5: Infrared spectra of (a) compound **1** and (b) compound **1** after heating up to 210°C and return to room temperature.

Fig 6: Crystallization of (a) ω-$VOPO_4$ at 430 °C in air and (b) $(VO)_2P_2O_7$ from 575 °C in N_2. The corresponding patterns calculated from their crystal structures are represented in green.

Scheme 1: Pathways to different vanadyl phosphates by thermal treatments of **1**

Table 1: Table 1: Hydrogen bonding geometry in **1**.

	D-H (Å)	H···A (Å)	D···A (Å)	<D-H···A> (°)
N1-H1N···Ow1$^{(i)}$	0.91(2)	2.04(2)	2.934(4)	171(4)
N1-H2N···O3	0.90(2)	2.06(2)	2.961(4)	177(5)
N1-H3N···O5$^{(ii)}$	0.90(2)	2.14(3)	3.007(4)	163(6)
N1-H4N···Ow1$^{(iii)}$	0.91(2)	1.98(2)	2.853(4)	161(4)
Ow1-H1W1···O5$^{(iv)}$	0.91(2)	2.13(4)	2.961(3)	151(5)
Ow1-H2W1···O4	0.92(2)	1.94(2)	2.851(3)	172(4)
Ow2-H1W2*···Ow1$^{(i)}$	0.863(7)*	1.958(3)	2.769(7)	155.9(5)
Ow2-H2W2*···O2$^{(v)}$	0.866(7)*	2.408(2)	3.151(7)	144.2(5)

Symmetry code : (i) x, 1+y, -1+z ; (ii) x, 1+y, z ; (iii) 1-x, 1-y, 1-z ; (iv) –x, -y, 1-z ; (v) 1+x, y, z.

* H atom at fixed position

Highlights

- The first ammonium vanadium oxalatophosphite has been synthesized hydrothermally.
- The layered structure of the compound has been established by a combined approach X-ray diffraction-Solid State NMR and is related to the structures of vanadium oxalato-phosphates.
- Adequate redox balance during the thermal decomposition of the ammonium vanadium oxalatophosphite allows the preparation of different active phases of catalytic vanadyl phosphate material.

Fig. 1

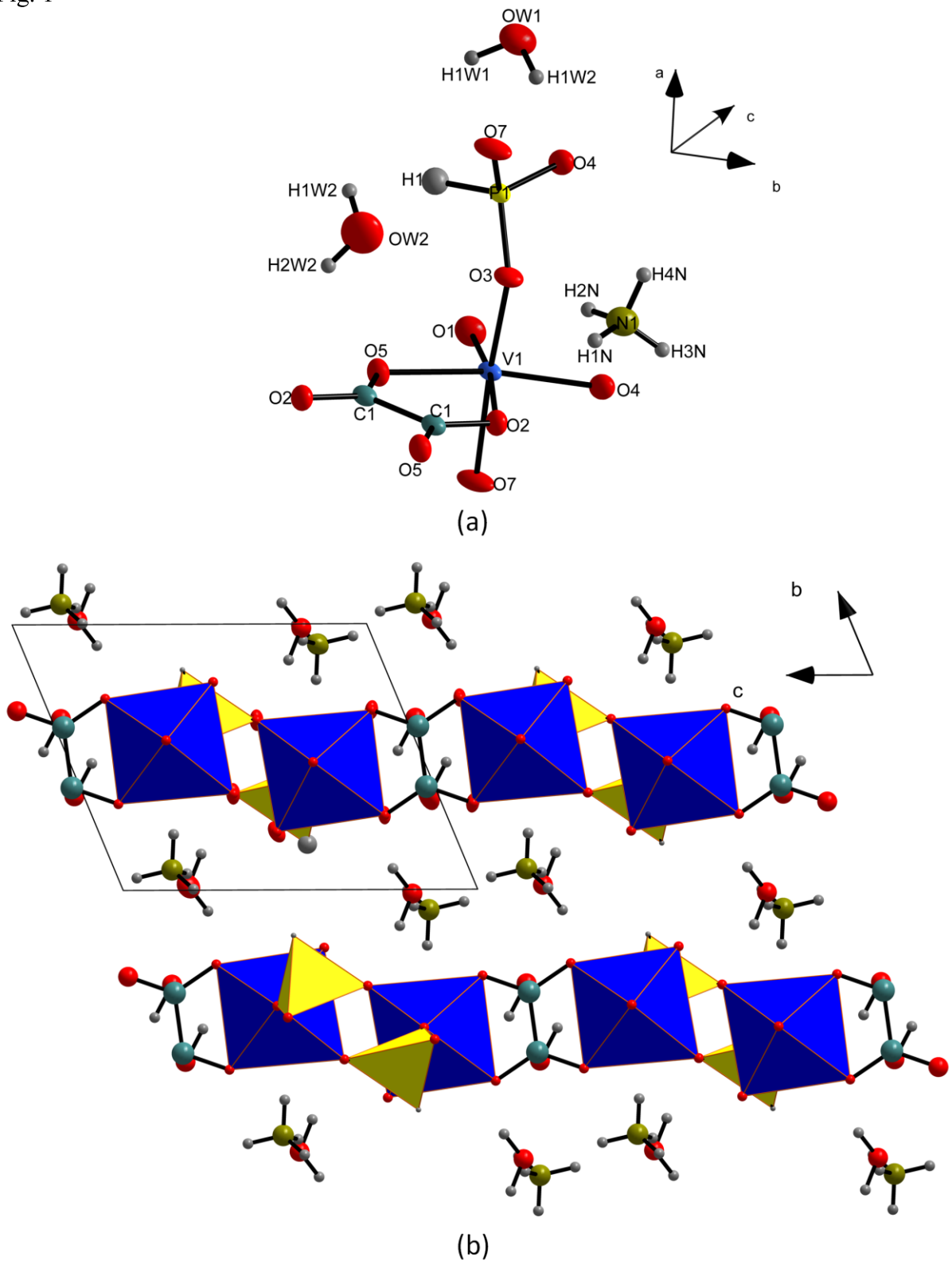

Fig. 2

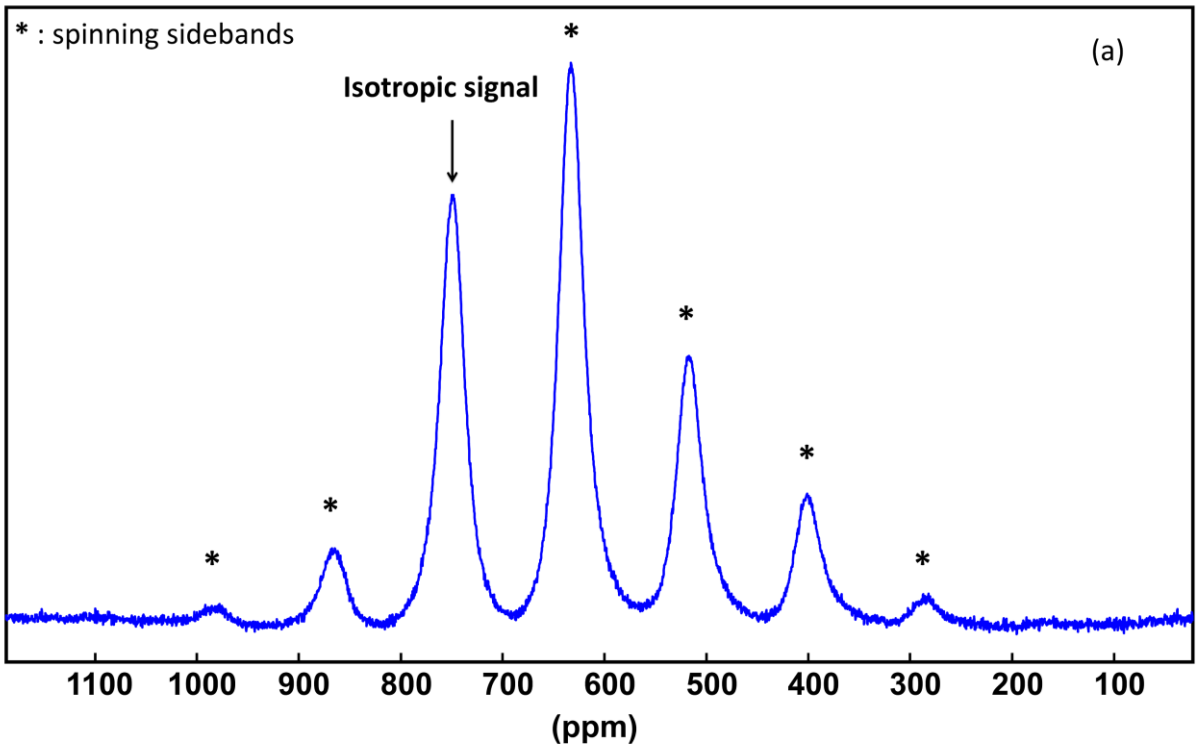

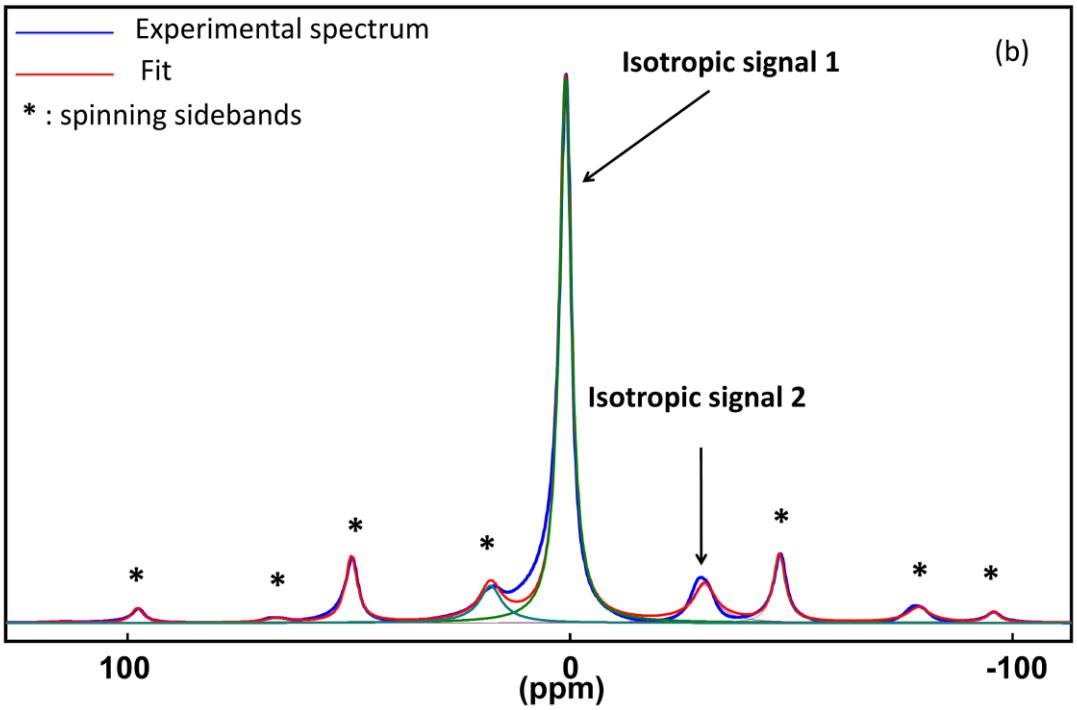

Fig. 3

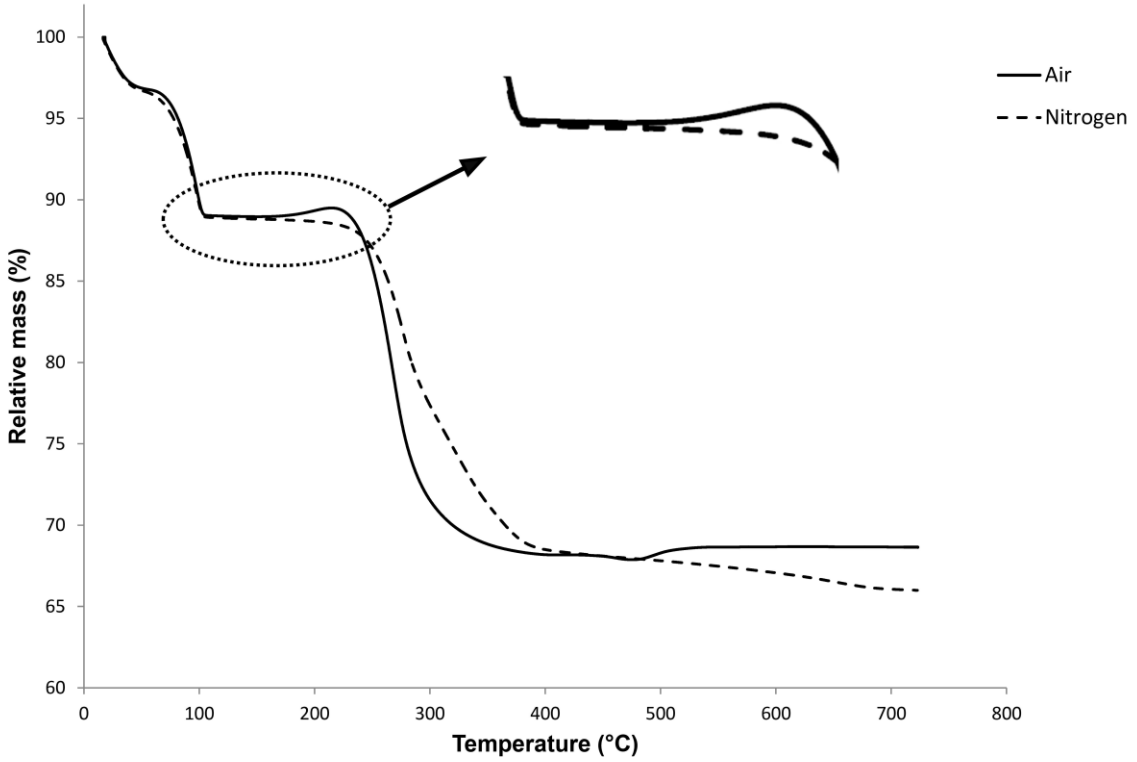

Fig. 4

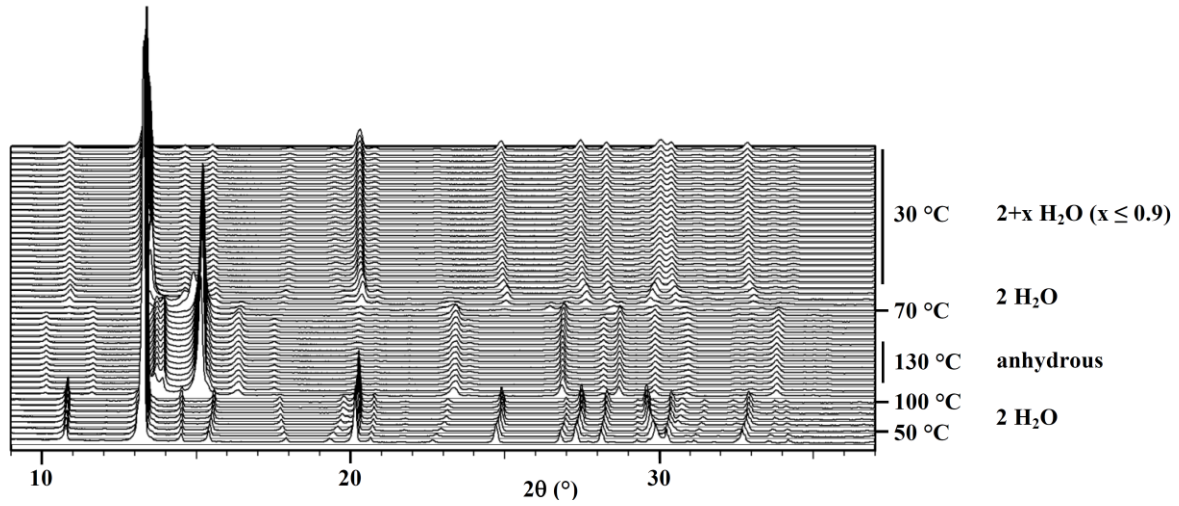

Fig. 5

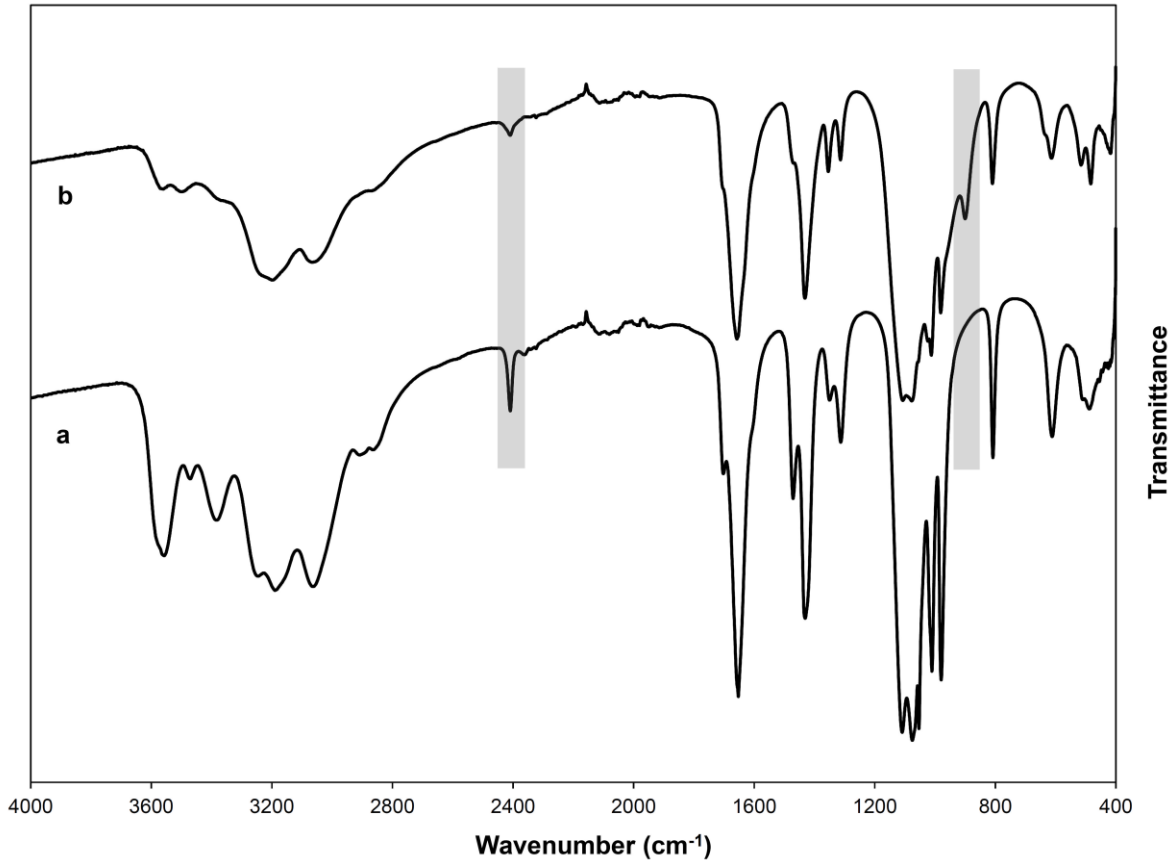

Fig. 6

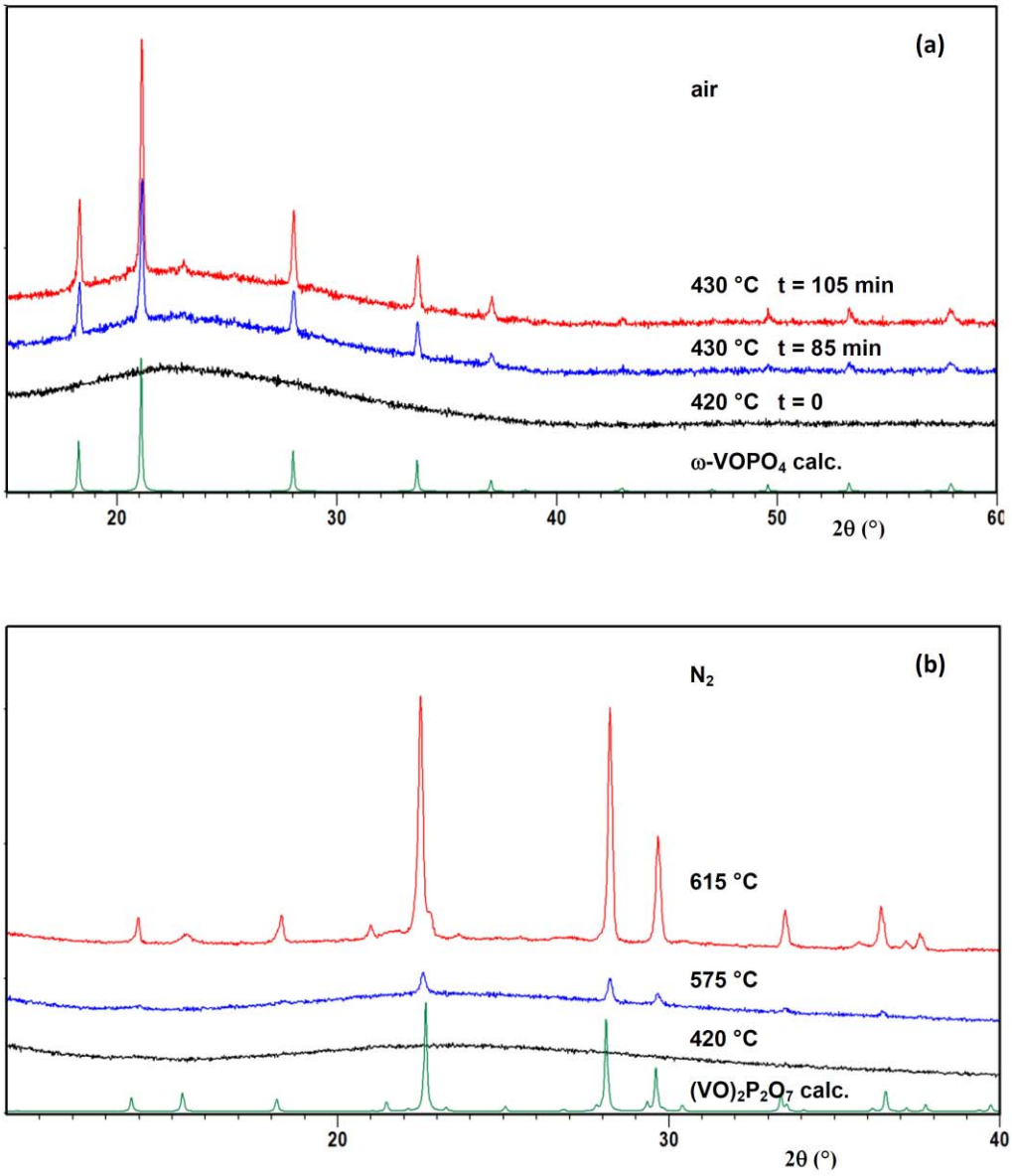

Graphical Abstract

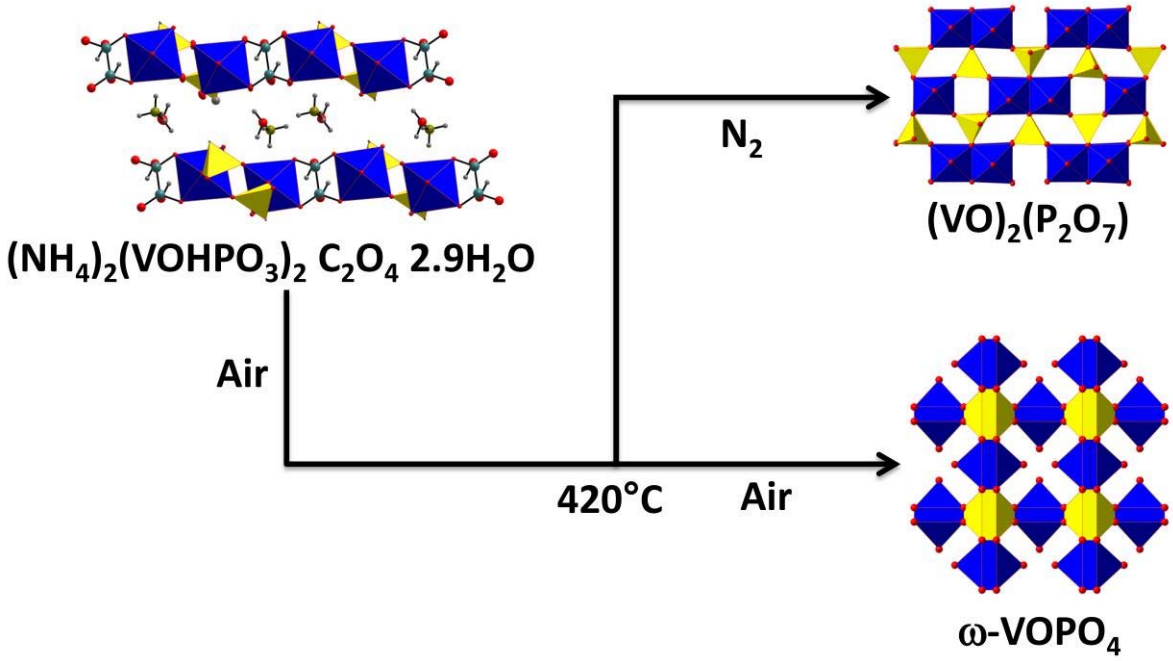

Scheme. 1